Mater. Res. Soc. Symp. Proc. Vol. 1182 © 2009 Materials Research Society 1182-EE16-03

Near-Field Radiation from Nano-Particles and Nano-Antennas Illuminated with a Focused Beam of Light

Kursat Sendur, Ahmet Sahinoz, Eren Unlu, Serkan Yazici, and Mert Gulhan
Sabanci University, Istanbul, 34956, Turkey.

ABSTRACT

The interaction of photons with metallic nanoparticles and nanoantennas yields large enhancement and tight localization of electromagnetic fields in the vicinity of nanoparticles. In the first part of this study, the interaction of a spherical nanoparticle with focused beams of various angular spectra is investigated. This study demonstrates that the focused light can be utilized to manipulate the near-field radiation around nanoparticles. In the second part of this study, the interaction between linearly and radially polarized focused light with prolate spheroidal nanoparticles and nano-antennas is investigated. Strong and tightly localized longitudinal components of a radially polarized focused beam can excite strong plasmon modes on elongated nanoparticles such as prolate spheroids. The effect of a focused beam on parameters such as the numerical aperture of a beam and the wavelength of incident light, as well as particle geometry and composition are also studied.

INTRODUCTION

The interaction of photons with metallic nanoparticles and nanoantennas is important to a number of emerging nanotechnology applications due to the large enhancement and tight localization of electromagnetic fields in the vicinity of nanoparticles and nanoantennas. This interaction has potential applications at the nanoscale, including near-field scanning optical microscopy [1], optical [2] and magneto-optical [3] high-density data storage, nano-lithography [4], bio-chemical sensing [5], nanoparticle-tweezers [6], and plasmonic solar cells [7]. The plasmon resonance of metallic nanoparticles is a well-studied field [8-9]. The effects of the wavelength, the surrounding medium, the composition, and the shape of the nanoparticle have been investigated in detail [10-11].

Although experimental studies in the literature have used both collimated and focused beams to excite surface plasmons [12-17], until recently the analytical and numerical models in the literature have only used simple plane waves to analyze this interaction. Recently, there has been increasing interest in understanding the interaction of a focused beam of light with a nanoparticle using both numerical and analytical techniques. Numerical techniques based on finite difference time-domain [18] and finite element method [19], as well as analytical techniques based on generalized Mie theory have been used [19-23] to analyze the interaction of a focused beam with a nanoparticle. Focused beam models have also been utilized for other nanostructures, such as nanowaveguides for potential utilization in high density data storage [24]. In a more recent study Mojarad et al. [25] used a radially polarized focused beam to tailor the localized surface plasmon spectra of nanoparticles.

In this study, we investigate the effect of the angular spectrum of a focused beam of light on the near-field radiation from spherical nanoparticles, prolate spheroidal nanoparticles, and dipole nano antennas. Focused beams with various angular specta are utilized in this study.

SPHERICAL NANOPARTICLES

To analyze the effect of the angular spectrum on the near-field radiation from a spherical nanoparticle, a silver nanoparticle is illuminated using a focused beam of light with small and large α. The focused beam propagates in the z-direction and is polarized in the x-direction. In Fig. 1, the electric field is computed at various wavelengths on the x-z cut-plane for a silver sphere with a 250 nm radius. The field distributions in Fig. 1 are normalized to the value of the incident intensity at the focus. At each wavelength, the field distribution $E_x(x,0,z)$ and $E_z(x,0,z)$ is plotted for α =5° and α =60°. A comparison of Figs. 1 (a) and (d) suggests that the field distribution at λ=400 nm for α =5° shows a significant difference compared to the results of α =60°. In Figs. 1 (a)-(f), deviations are observed at other wavelengths as well. The E_y component is negligible for the solutions. The impact of altering the angular spectrum is more drastic for the E_z component, as shown in Figs. 1 (g)-(l). For example, when the angular spectrum is narrowly distributed along the direction of propagation, as shown in Fig. 1 (i), two stronger lobes are observed at the back of the spherical particle. As α is increased, and therefore the angular spectrum is widened, the stronger lobes are moved from the back of the particle to the front of the particle, as shown in Fig. 1 (l). This was achieved without changing the frequency, geometry, or composition of the particle. Suppressing strong near-field radiation lobes and enhancing weaker radiation lobes is possible by altering the angular spectrum.

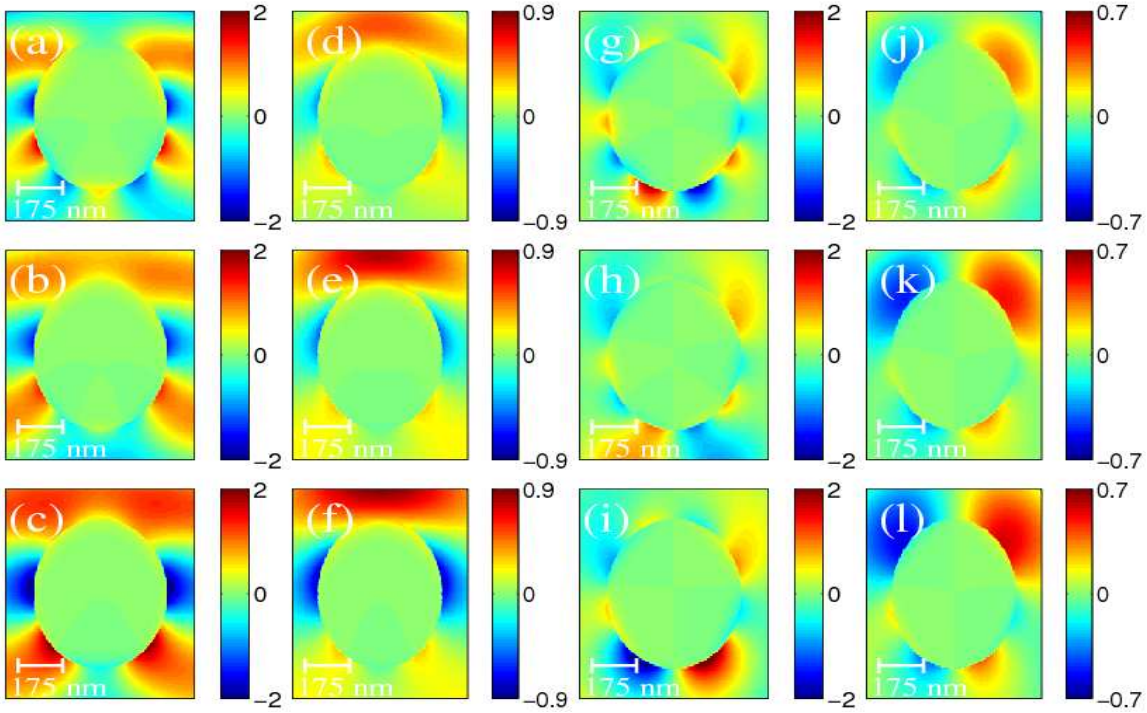

Figure 1. $E_x(x,0,z)$ and $E_z(x,0,z)$ on x-z for various [α,λ]: (a) $E_x(x,0,z)$ for [5,400], (b) $E_x(x,0,z)$ for [5,500], (c) $E_x(x,0,z)$ for [5,600], (d) $E_x(x,0,z)$ for [60,400], (e) $E_x(x,0,z)$ for [60,500], (f) $E_x(x,0,z)$ for [60,600], (g) $E_z(x,0,z)$ for [5,400], (h) $E_z(x,0,z)$ for [5,500], (i) $E_z(x,0,z)$ for [5,600], (j) $E_z(x,0,z)$ for [60,400], (k) $E_z(x,0,z)$ for [60,500], and (l) $E_z(x,0,z)$ for [60,600],

PROLATE SPHEROIDAL NANOPARTICLES

In this section, the impact of the angular spectrum distribution of the incident radially polarized beam on the near-field radiation of spheroidal nanoparticles is studied. In Fig. 2 (a), a schematic illustration of a prolate spheriodal nanoparticle and the incident radially polarized focused beam is provided. In Fig. 2 (b), the total intensity profile is plotted on the x-z plane, which passes through the center of a gold prolate spheroid particle with a major/minor axis ratio of 5. In Fig. 3, $|E|^2$ distributions for a gold prolate spheroid are given for various half-beam angles. In this figure, the prolate spheroids are illuminated with a radially focused beam with half-beam angles α=15°, α=30°, α=45°, and α=60°. The field distributions in Figs. 2 and 3 are normalized to the value of the incident intensity at the focus. The results suggest that the electric field distribution does not change as the half-beam angle is increased. The amplitude of the near-field electric field distribution, however, increases as the half-beam angle is increased. The angular spectrum of the incident beam is tight for α=15°, becoming wider as the half beam angle is increased. Therefore, the incident wave amplitude onto the particle increases as the half-beam angle increases. As a result of increasing the incident field amplitude, the scattered field amplitude also increases, as shown in Fig. 3.

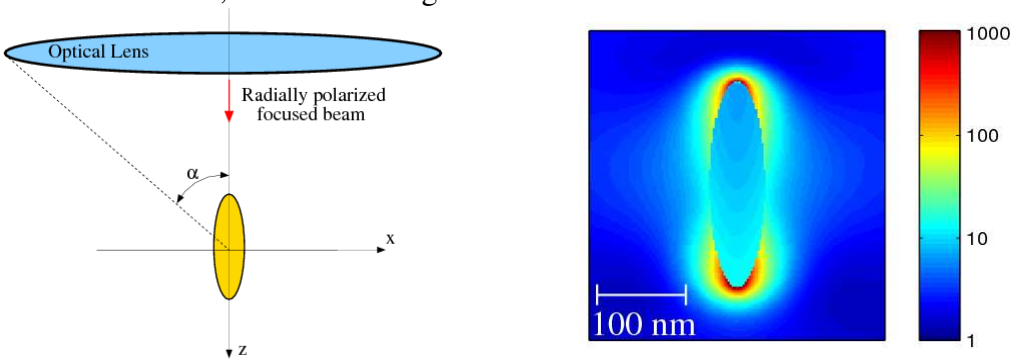

(a) (b)

Figure 2. (a) A schematic illustration of a prolate spheriodal nanoparticle and the incident radially polarized focused beam. (b) $|E|^2$ distribution on the x-z cut plane for a gold prolate spheroid particle of major axis radius of 100 nm and a major/minor axis ratio of 5 illuminated with a radially polarized focused light at λ =700 nm.

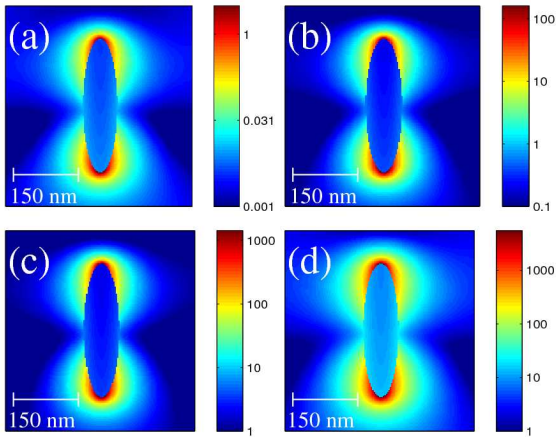

Figure 3. $|E|^2$ distributions for a gold prolate spheroid. The distributions are given for various half-beam angles: (a) α=15°, (b) α=30°, (c) α=45°, and (d) α=60°.

NANOANTENNAS

Figure 4 illustrates the focused incident $|E^i|^2$ distributions onto the dipole nano-antennas. The fields are plotted at the focal plane x-y for various half-beam angles. For small α, the field distribution is similar to that of a plane wave. As the α increases, the beam becomes more tightly focused. In Fig. 5, the total $|E^t|^2$ distribution for a dipole antenna is shown on the x-z cut-plane plane when it is illuminated with the focused beams shown in Fig. 4. For this particular simulation, the sizes of the antenna are L= 110, T= 20, W= 20, and G= 20 nm. In this simulation, the incident focused beam is polarized in the x-direction, and propagates in the negative z-direction. The wavelength of the incident light is 850 nm. The antenna is placed at the focus of the incident beam, which is also the global origin for the simulations. The peak value of the graphs in Fig. 5 represents the intensity enhancement, which is defined as

$$\text{Intensity Enhancement} = \frac{\left|E^t(0,0,0)\right|^2}{\left|E^i(0,0,0)\right|^2} \tag{1}$$

In other words, total intensity $|E^t|^2$ at the antenna gap center is normalized to the value of the incident intensity $|E^i|^2$ at the focus. The results in Fig. 5 show a confined electric field close to the gap region of the antenna. Also, a large electric field enhancement is observed for all the half-beam angle values α. The intensity enhancement at the center of the antenna is about 1200 for small α. The intensity enhancement slowly reduces to 1100 as α is increased.

The results in Fig. 5 indicate that the contribution from the rays with large incident angles is less than the contribution from the rays with small incident angles. To provide further evidence for this observation, the incident beam is separated into angular spectral bands. The contribution from each spectral band is then calculated separately. To achieve this, the incident beam is passed through an angular band-pass filter as shown in Fig. 6. The filter supresses the $\theta<\theta_{min}$ and $\theta>\theta_{max}$ part of the angular spectrum. In this calculation, spectral bands with 5° intervals are considered, which corresponds to $\theta_{min} = \theta_{min+}5°$. Intensity enhancement is plotted as a function of θ_{min} in Fig. 7. The results suggest that the intensity enhancement due to rays with large incident angles is less than the intensity enhancement from the rays with small incident angles.

As we mentioned above, the results in Fig. 5 indicates that the intensity enhancement is almost preserved as α increases. The output power, however, not only depends on the intensity enhancement but also on the intensity of the incident focused beam. As shown in Fig. 8, the intensity of the incident focused beam $|E^i(0,0,0)|^2$ increases with increasing α. The incident beam becomes more tightly focused with increasing α, which increases the incident electric field intensity, as shown in Fig. 8. As a result, the output intensity increases with increasing α. This suggests that significant gains can be achieved by increasing the α, despite a small reduction in the transmission efficiency.

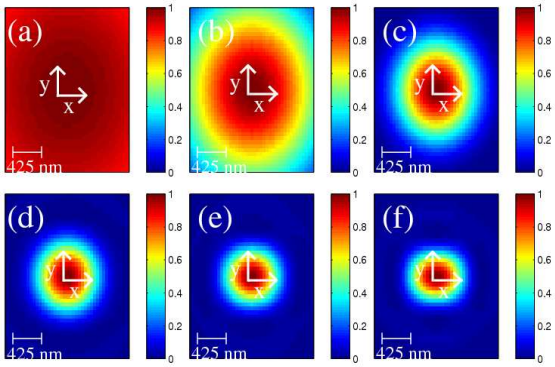

Figure 4. Incident $|E|^2$ distribution in the absence of nanoantennas. The fields are plotted at the focal plane x-y for: (a) α =5°, (b) α =15°, (c) α =30°, (d) α =45°, (e) α =60°, and (f) α =75°.

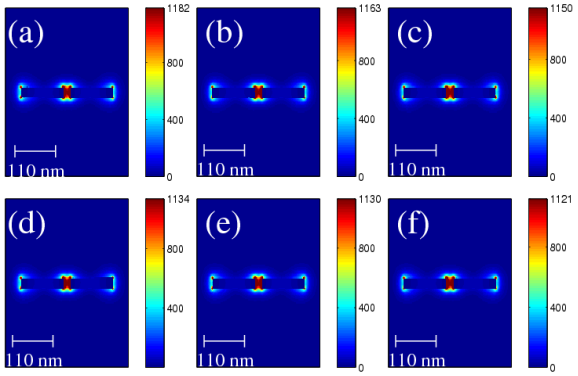

Figure 5. Total $|E|^2$ distribution in the presence of nano-antennas. The fields are plotted on the x-y cut plane for: (a) α =5°, (b) α =15°, (c) α =30°, (d) α =45°, (e) α =60°, and (f) α =75°.

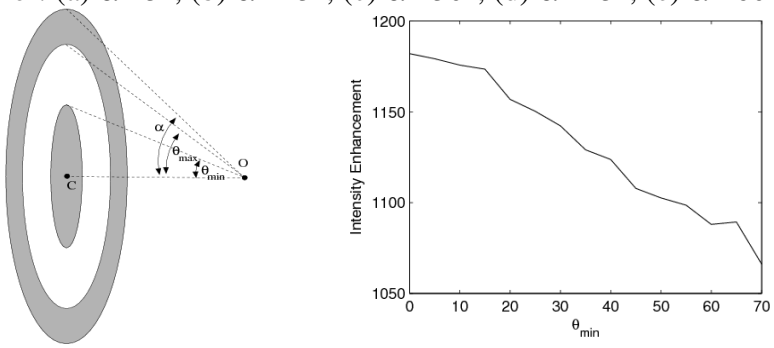

(a) (b)

Figure 6. (a) A band-pass filter supresses the $\theta<\theta_{min}$ and $\theta>\theta_{max}$ part of the angular spectrum. (b) Intensity enhancement as a function of θ_{min}. The cut-off angle is selected as $\theta_{min} = \theta_{min+}5°$.

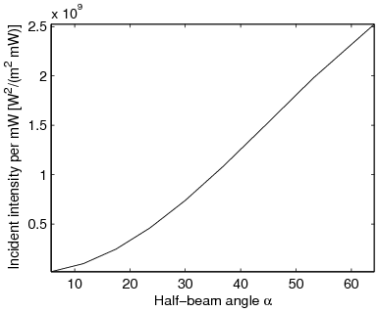

Figure 7. Incident intensity per mW incident power as a function of α for λ=850 nm.

CONCLUSIONS

In summary, it has been demonstrated that the near-field radiation from a spherical particle can be manipulated by adjusting the angular spectrum of an incident focused beam. On the other hand, for prolate spheroids the electric field distribution does not change as the half-beam angle is increased. The amplitude of the near-field electric field distribution, however, increases as the half-beam angle is increased. For nano-antennas the intensity enhancement is almost preserved as α increases. For more tightly focused beams, the output intensity increases with increasing α. This suggests that for nano-antennas, significant gains can be achieved by increasing the α despite a small reduction in the transmission efficiency.

REFERENCES

1. A. Hartschuh, E. J. Sanchez, X. S. Xie, and L. Novonty, Phys. Rev. Lett. **90**, 095503 (2003).
2. T. D. Milster, Optics and Photonics News **16**, 28–32 (2005).
3. R. E. Rottmayer, S. Batra, D. Buechel, W. A. Challener, J. Hohlfeld, Y. Kubota, L. Li, B. Lu, C. Mihalcea, K. Mountfield, K. Pelhos, C. Peng, T. Rausch, M. A. Seigler, D. Weller, and X. Yang, IEEE Trans. Magn. **42**, 2417–2421 (2006).
4. L. Wang and X. Xu, J. Microsc. **229**, 483–489 (2008).
5. B. Liedberg, C. Nylander, I. Lundstroem, Sens. Actuators **4**, 299–304 (1983).
6. Q. Zhan, Opt. Express **12**, 3377–-3382 (2004).
7. K. R. Catchpole and A. Polman, Opt. Express **16**, 21793 (2008).
8. J. Crowell and R. H. Ritchie, Phys. Rev. **172**, 436–440 (1968).
9. M. Kerker, Appl. Optics **18**, 1180–1189 (1979).
10. K. L. Kelly, E. Coronado, L. L. Zhao, and G. C. Schatz, J. of Phys. Chem. B **107**, 668–677 (2003).
11. O. Sqalli, I. Utke, P. Hoffmann, and F. Marquis-Weible, J. Appl. Phys. **92**, 1078–1083 (2002).
12. H. Kano, D. Nomura, and H. Shibuya, Appl. Opt. **43**, 2409–2411 (2004).
13. H. Kano, S. Mizuguchi, and S. Kawata, J. Opt. Soc. Am. B **15**, 1381–1386 (1998).
14. A. Bouhelier, F. Ignatovich, A. Bruyant, C. Huang, G. Colas des Francs, J.-C. Weeber, A. Dereux, G. P. Wiederrecht, and L. Novotny, Opt. Lett. **32**, 2535–2537 (2007).
15. A. V. Failla, H. Qian, H. Qian, A. Hartschuh, and A. J. Meixner, Nano Lett. **6**, 1374–1378 (2006).
16. A. V. Failla, S. Jager, T. Zuchner, M. Steiner, and A. J. Meixner, Opt. Express **15**, 8532–8542 (2007).
17. T. Zuchner, A. V. Failla, A. Hartschuh, and A. J. Meixner, J. Microsc. **229**, 337–343 (2007).
18. W. A. Challener, I. K. Sendur, and C. Peng, Opt. Express **11**, 3160–3170 (2003).
19. K. Sendur, W. Challener, and O. Mryasov, Opt. Express **16**, 2874–2886 (2008).
20. J. Lerme, G. Bachelier, P. Billaud, C. Bonnet, M. Broyer, E. Cottancin, S. Marhaba, and M. Pellarin, J. Opt. Soc. Am. A **25**, 493–514 (2008).
21. N. M. Mojarad, V. Sandoghdar, and M. Agio, J. Opt. Soc. Am. B **25**, 651–658 (2008).
22. N. J. Moore and M. A. Alonso, Opt. Express **16**, 5926–5933 (2008).
23. C. J. R. Sheppard and P. Torok, J. Mod. Opt. **44**, 803–818 (1997).
24. K. Sendur, C. Peng, and W. Challener, Phys. Rev. Lett. **94**, 043901 (2005).
25. N. M. Mojarad and M. Agio, Opt. Express **17**, 117–122 (2008).